# Anomalous absorption in ECRH experiments due to the parametric low-threshold excitation of localized UH waves

*Alexei Yu. Popov*, *Evgeniy Z. Gusakov*

Ioffe Institute, St. Petersburg 194021, Russia

**Abstract.** We describe the theoretical model which interprets the anomalous phenomena, *i.e.* the generation of backscattering signal observed in the ECRH experiments at TEXTOR, TCV, TJ-II, ASDEX-UG, LHD and FTU, as a consequence of the excitation of the parametric decay instability (PDI) leading to anomalous damping of the pump wave. The PDI power-threshold is shown to be extremely low due to the localization of both or one daughter upper hybrid (UH) waves in presence of a nonmonotonic (hollow) density profile, which is often observed in the ECRH experiments due to the magnetic island or the density pump-out effect. In the case of the extraordinary wave pump the model predicts substantial (up to 25%) anomalous absorption in the electron channel and explains the anomalous ion acceleration by the generation of secondary low frequency waves which directly transfer the pump power to the ion component. The possibility of anomalous absorption of the O-mode pump in the ECRH experiment due to the parametric excitation of trapped UH wave is also discussed and the anomalous absorption rate at the 10% level is predicted.

## 1 Introduction

Electron cyclotron resonance heating (ECRH) and current drive is widely used in toroidal plasmas and is considered for application in ITER for heating and neoclassical tearing mode control. The parametric decay instabilities (PDIs), which can accompany the ECRH experiments, are believed to be deeply suppressed by the huge energy loss of daughter waves from the decay region, according to the predictions of theory developed in 80$^{th}$ [1]. However, during the last decade numerous ECRH experiments performed at TEXTOR, TCV, TJ-II, ASDEX-UG, LHD, T-10 and FTU [2-13] have demonstrated excitation of the anomalous phenomena. The clearest evidence of the nonlinear phenomena excitation was obtained at TEXTOR [2, 3] where the strong backscattering signals down–shifted in frequency and amplitude modulated at the frequency of magnetic island were observed. A convincing demonstration of the anomalous ion acceleration during the ECRH pulse under conditions when the energy exchange between the ion and electron components is negligible was obtained at TCV [4,5].

In the present paper we describe the theoretical model taking into account, as distinct from the conventional theory [1], the presence of a non-monotonic density profile, which always exists on the discharge axis or may be present due to the magnetic island or the density pump-out effect. We interpret the generation of backscattering signal and the anomalous ion heating, as a result of secondary nonlinear processes that accompany a primary low – threshold two–upper-hybrid (UH) – plasmon PDI of the pump X2-mode wave. The threshold of primary PDI is shown [14, 15] to be smaller than the one predicted in [1] due to the trapping of at least one UH wave in presence of the non-monotonic density profile. The primary PDI appears to be absolute due to the finite-size of a pump beam. Its growth enhancing the UH wave fluctuations from the thermal noise level is saturated in our theory due to both the secondary decays of the daughter UH wave that leads to excitation of the secondary UH and ion Bernstein (IB) waves [16] and the pump wave depletion. The threshold of this spontaneous parametric frequency down-conversion can be easily overcome for the radially trapped secondary UH waves. The couplings of different daughter UH waves are responsible in the theory for the generation of backscattering signals [17]. This mechanism appears capable of reproducing the fine details of the frequency spectrum of anomalously backscattered X wave and the absolute value of the observed backscattering signal in TEXTOR experiment. It also predicts substantial (up to 25%) anomalous absorption in the electron channel and explains the anomalous ion heating at TCV by the generation of secondary IB waves, which directly transfer the pump power to the ion component.

The results of a model experiment, demonstrating strong anomalous absorption of the X-mode pump in a plasma filament due to the two-plasmon decay [18] and thus confirming the theory, are discussed.

The possibility of anomalous absorption of the O-mode pump in the ECRH experiment due to parametric excitation of the trapped UH wave [19,20] is discussed as well.

* Corresponding author: a.popov@mail.ioffe.ru

© The Authors, published by EDP Sciences. This is an open access article distributed under the terms of the Creative Commons Attribution License 4.0 (http://creativecommons.org/licenses/by/4.0/).

## 2 Model

We assume that the three-wave nonlinear interaction leading to the low-threshold PDI excitation occurs in a small volume in the vicinity of a local maximum of plasma density profile illuminated by the pump beam where the daughter UH waves/wave are localized. Therefore, it seems to be reasonable to utilize throughout the paper, describing different PDIs, the Cartesian coordinate system $(x,y,z)$ with its origin located at the local maximum of the UH frequency profile, the *x*-axis directed along the flux coordinate and (*y,z*) imitating accordingly the coordinates perpendicular to and aligned with the magnetic field line on the magnetic surface.

### 2.1. Two-UH-plasmon parametric decay of an extraordinary wave

We start with consideration of the low-power threshold two-UH-plasmon decay of a beam of the extraordinary (X) waves

$$\mathbf{E}=\mathbf{e}_0\frac{A_0}{2}\exp\left(i\int_{-\infty}^{x}k_x(\omega_0,x')dx'-i\omega_0 t\right)+c.c. \quad (1)$$

propagating perpendicular to the magnetic surface along the inhomogeneity direction and its saturation owing to the pump depletion and the cascade of secondary decays. In (1) $\mathbf{e}_0=i\mathbf{e}_x g(\omega_0)/\varepsilon(\omega_0)+\mathbf{e}_y$ is the polarization vector, $k_x\simeq\omega_0/c\sqrt{\varepsilon-g^2/\varepsilon}$ is the local wavenumber, $A_0$ is the slowly varying amplitude, $\varepsilon,g$ stand for the components of the cold-plasma dielectric tensor. A set of equations describing the two-step cascade of decays reads

$$\begin{aligned}
&\left(\frac{\partial^2}{\partial x^2}+k_x^2(\omega_0)\right)A_0=\frac{\omega_0^2}{c^2}\kappa_p^2\frac{\varphi_1^*\varphi_2}{H}\\
&\hat{D}(\varphi_1)=\kappa_p^2\frac{A_0^*}{H}\varphi_2-\kappa_s^2\frac{|e|}{T_e}\varphi_1'^*\varphi_2'\\
&\hat{D}(\varphi_2)=\kappa_p^2\frac{A_0}{H}\varphi_1 \quad (2)\\
&\hat{D}(\varphi_1')=\kappa_s^2\frac{|e|}{T_e}\varphi_1^*\varphi_2'\\
&\hat{D}(\varphi_2')=\kappa_s^2\frac{|e|}{T_e}\varphi_1\varphi_1'
\end{aligned}$$

where $\varphi_{1,2}$ are the potentials of primary UH waves, $\varphi'_{1,2}$ are the potentials of secondary UH and ion Bernstein (IB) waves and $\kappa^2_{p,s}$ are the coupling coefficients for both decays presented explicitly in [21]. In weakly inhomogeneous plasma the integral operators $\hat{D}$ are taking the following form:

$$\begin{aligned}
&\hat{D}(\varphi)=\int_{-\infty}^{t}\int_{-\infty}^{\infty}dt'd\mathbf{r}'D(t-t',\mathbf{r},\mathbf{r}')\varphi(\mathbf{r}',t'),\\
&D(t-t',\mathbf{r},\mathbf{r}')=\int_{-\infty}^{\infty}\frac{d\mathbf{q}d\omega}{(2\pi)^4}D(\omega,\mathbf{q},\mathbf{r}+\mathbf{r}')e^{i\mathbf{q}(\mathbf{r}-\mathbf{r}')-i\omega(t-t')}
\end{aligned} \quad (3)$$

with their kernel $D(\omega,\mathbf{q})=q^2+\chi_e+\chi_i$ being the local dispersion function of the corresponding electrostatic waves [22], obtained in the homogeneous plasma theory and $\chi_e$, $\chi_i$ standing for the familiar expressions of the electron and ion susceptibilities

$$\chi_j=\frac{2\omega_{pj}^2}{\upsilon_{tj}^2}\left(1-\frac{\omega}{q_z\upsilon_{tj}}\sum_{m=-\infty}^{\infty}Z\left(\frac{\omega-m\omega_{cj}}{q_z\upsilon_{tj}}\right)\exp\left(-\frac{q_\perp^2\upsilon_{tj}^2}{2\omega_{cj}^2}\right)I_m\left(\frac{q_\perp^2\upsilon_{tj}^2}{2\omega_{cj}^2}\right)\right) \quad (4)$$

In (4) $j$=*e,i*, $q_{\perp,z}$ are the wavenumber components perpendicular to and along the magnetic field, $\upsilon_{te,i}$ are the electron and ion thermal velocities, $\omega_{ce,i}$ and $\omega_{pe,i}$ are the electron and ion cyclotron and Langmuir frequencies, $I_m$ is the modified Bessel function of the first kind and $Z(\xi)=2\exp(-\xi^2)\int_0^{\xi}\exp(t^2)dt-i\sqrt{\pi}\exp(-\xi^2)$. In (2) we have assumed that only one primary UH wave experience frequency down-conversion. Then, we assume the nonlinear coupling is weak. This allows utilizing the perturbation theory approach [23], in the first step of which we drop all the RHS of equations (2) and seek the solutions of the homogeneous wave-equations. In particular, the trapped UH waves potentials are derived by means of the WKB approximation as

$$\begin{aligned}
&\varphi_{1,2}(\mathbf{r},t)=\phi_{n,m}(\mathbf{r})\exp(iq_y y\pm i\omega_{n.m}t)/2+c.c.,\\
&\varphi_2'(\mathbf{r},t)=\phi_p(\mathbf{r})\exp(-i\omega_p t)/2+c.c.
\end{aligned} \quad (5)$$

where $\omega_m=\omega_0-\omega_n$, $\omega_1'=\omega_n-\omega_p$, *c.c.* stands for the term derived from the first one by the complex conjugation,

$$\phi_n=\frac{C_n\exp\left(i\int_{x_{nl}^*}^{x}q_{nx}^{+}d\xi-i\frac{\pi}{4}\right)}{\sqrt{L_n^{+}(x)}}+\frac{C_n\exp\left(i\int_{x_{nl}^*}^{x}q_{nx}^{-}d\xi+i\frac{\pi}{4}\right)}{\sqrt{L_n^{-}(x)}} \quad (6)$$

is the eigenfunction, $C_n=const$, $q_{nx}^{\pm}$ is a root of the local UH wave dispersion relation, $L_n^{\pm}$ stands for the optical length of the wave path between two turning points $(x_{nl}^*,x_{nr}^*)$. The frequencies $\omega_n$, $\omega_m$ and the poloidal wave-number $q_y^{n,m}$ obey simultaneously the quantization conditions. The frequency of secondary UH wave $\omega_p$ obeys the quantization condition as well

$$\sum_{s=\pm}\int_{x_{pl}^*}^{x_{pr}^*}q_{jx}^{s}(\omega_p,\xi)d\xi=\pi(2p+1) \quad (7)$$

Equation (6) describes the UH wave localized in the $x$-direction at the maximum of the UH frequency profile.

In the second step of the perturbation procedure we take into consideration the nonlinear interactions and the pump energy loss due to the UH plasmons excitation. We utilize the envelope amplitude method and keep in mind the boundary condition for the pump wave

$$A_0(\mathbf{r})\big|_{x\to-\infty}=\sqrt{\frac{8P_0}{w^2\upsilon_{gx}}}\exp\left(-\frac{y^2+z^2}{2w^2}\right) \quad (8)$$

with $\upsilon_{gx}(x)$, $P_0$, $w$ being the wave group velocity, pump power and beam width. Finally we get

$$\begin{aligned}
&\left(\frac{\partial}{\partial t}-u_n\frac{\partial}{\partial y}+i\Lambda_n\frac{\partial^{=2}}{\partial z^2}\right)a_n=\nu_0^*\exp\left(-\frac{y^2+z^2}{2w^2}\right)a_m\\
&-\left(\nu_d^*\frac{|a_m|^2}{a_T^2}+\nu_s^*\frac{|a_p|^2}{a_T^2}\right)a_n\\
&\frac{\partial a_m}{\partial t}+u_m\frac{\partial a_m}{\partial y}-i\Lambda_m\frac{\partial^2 a_m}{\partial z^2}=\nu_0\exp\left(-\frac{y^2+z^2}{2w^2}\right)a_n-\nu_d\frac{|a_n|^2}{a_T^2}a_m
\end{aligned}$$

$$\frac{\partial a_p}{\partial t}+u_p\frac{\partial a_p}{\partial y}-i\Lambda_p\frac{\partial^2 a_p}{\partial z^2}=\nu_s\frac{|a_n|^2}{a_{\mathrm{T}}^2}a_p \qquad (9)$$

where

$$a_{n,m,p}=\left|C_{n,m,p}\right|\left(\omega_{n,m,p}<D_{n,m,p\omega}>/16\pi\right)^{1/2}, \qquad (10)$$

$<D_{n,m,p\omega}>=<\partial D/\partial\omega|_{\omega_{n,m,p}}>$, $<...>$ stands for averaging over the localization region of the corresponding UH plasmons

$$<...>=\int_{-\infty}^{\infty}dx...\left|\phi_{n,m,p}(x)\right|^2, \qquad (11)$$

$|a_{n,m,p}|^2$ yield their energy, $u_{n,m,p}=<\partial D/\partial q_y|_{\omega_{n,m,p}}>$ are the convective velocities in the poloidal direction, $\Lambda_{n,m,p}=<\partial^2 D/\partial(2q_z^2)|_{\omega_{n,m,p}}>$ are the diffraction coefficients along the magnetic field,

$$\nu_0=i\sqrt{\frac{2P_0}{w^2H^2\upsilon_{gx}}}\int_{-\infty}^{\infty}dx\frac{\kappa^2(x)\phi_n^*(x)\phi_m(x)}{\sqrt{<D_{1\omega}><D_{2\omega}>}}\exp\left(-i\int^x k_x(x'')dx''\right),$$

$$\nu_d=\frac{4\pi a_{\mathrm{T}}^2}{H^2c}\times$$

$$\int_{-\infty}^{\infty}dx\int_{-\infty}^{x}dx'\frac{\kappa^2(x)\kappa^2(x')}{<D_{1\omega}><D_{2\omega}>}\phi_n(x)\phi_m^*(x)\phi_n^*(x')\phi_m(x')\exp\left(i\int_{x'}^{x}k_x(x'')dx''\right),$$

$$\nu_s=\frac{4\pi a_{\mathrm{T}}^2}{H^2}\left[\frac{c\omega_{pe}^2}{\left(\omega_1^2-\omega_{ce}^2\right)\left(\omega_1'^2-\omega_{ce}^2\right)}\frac{\omega_1\omega_1'}{|\omega_{ce}|}\right]_{x_m}\times$$

$$\int_{-\infty}^{\infty}dx\frac{q_{1x}(x)q_{1x}'(x)q_{Ix}^2(x)}{\sqrt{<D_{1\omega}(x)><D_{1\omega}'(x)>}}\frac{\phi_n^*(x)\phi_p'^*(x)}{\sqrt{D_{lq}(x)}}\times$$

$$\int_{x}^{\infty}dx'\frac{q_{1x}(x')q_{1x}'(x')q_{Ix}^2(x')}{\sqrt{<D_{1\omega}(x')><D_{1\omega}'(x')>}}\frac{\phi_n(x')\phi_p'(x')}{\sqrt{D_{lq}(x')}}\exp\left(i\int_{x'}^{x}q_{Ix}(x'')dx''\right)$$

are the coupling coefficients [21] describing the primary ($\nu_0$) and secondary ($\nu_s$) decays, the pump wave depletion ($\nu_d$) and

$$a_{\mathrm{T}}=\sqrt{T_{\mathrm{e}}/(\pi w^2)} \qquad (12)$$

Further, we analyze (9) analytically and then solve numerically. We start with consideration of the growth-rates of primary and secondary decays and get an estimation of the daughter wave saturation levels based on the energy-balance formulation. For the conditions under consideration the convective energy losses of the primary and secondary UH plasmons from the decay layer in the poloidal direction are much smaller than their energy losses in a form of diffraction in the toroidal direction, *i.e.* $u_{n,m,p}w/\Lambda_{n,m,p,}<<1$ and $\Lambda_{n,m,p}\approx\Lambda$. In this case the growth-rate of the primary two-UH-plasmon decay can be evaluated on the basis of analysis carried out in [14] as

$$\gamma=\sqrt{|\nu_0|^2-\left(\pi(2\zeta+1)/2w\right)^4\Lambda^2} \qquad (13)$$

with $\zeta$ being the unstable eigenmode number. As soon as the energy of primary plasmons growing exponentially reaches a level which exceeds the threshold of secondary decay instability, the energy of secondary plasmons has to start growing as well. Eventually, the nonlinear system relaxes to the stationary regime in which the saturation level of primary plasmons number $|a_n^s|^2$ can be evaluated from a condition indicating saturation of the secondary decay described by the last equation in (9). Namely, the growth rate $\nu_s|a_1|^2$ of this decay should be compensated by the secondary UH plasmon diffractive loss rate from the pump beam spot, characterized by a typical time scale $\tau=\pi w^2/\Lambda$. The corresponding level is given by

$$\left|a_n^s\right|^2\approx a_{\mathrm{T}}^2/(\tau\nu_s) \qquad (14)$$

The number of the primary plasmons $|a_m^s|$ in the saturation regime could be estimated using the second equation of (9) as

$$|a_m^s|^2\approx\frac{|\nu_0|^2}{\tau^{-2}+|\nu_d|^2|a_n^s|^4/a_{\mathrm{T}}^4}|a_n^s|^2 \qquad (15)$$

The energy of secondary plasmons $|a_p^s|^2$ saturates at a level balancing the nonlinear pumping rate $\nu_0|a_m|$ and the loss rate due to the secondary decay of first ($a_n$) primary UH wave $\nu_s\left|a_p\right|^2|a_n|$. This saturation level can be estimated as

$$|a_p^s|^2\approx\frac{a_{\mathrm{T}}^2}{|\nu_s|}\frac{|\nu_0|^2}{\sqrt{\tau^{-2}+|\nu_d|^2|a_n^s|^4/a_{\mathrm{T}}^4}}. \qquad (16)$$

Then, we solve (9) numerically in a 2D box $2y_B\times2z_B$ assuming the periodic boundary conditions and an initial thermal-noise-level of the UH waves. The imposed boundary conditions imitate the toroidal geometry and describe the multiple transitions of UH plasmons through the 2D box. However, it is worth noting that equations (9) were derived ignoring the magnetic field poloidal dependence. Thereby, the meaningful solution of (9) is an intermediate asymptotic dependence valid at the time much less than the transition time of the daughter waves through the 2D box. We assume the initial thermal noise level (12) of all plasmons and use the parameters $w=1$ cm, $\mathrm{T_e}=600$ eV, $\mathrm{P_0}=600$ kW which correspond to the TEXTOR experimental conditions. The results of numerical solution of equations (9) are shown in Fig. 1 where the temporal evolution of the average energy of different daughter plasmons in the spot $<|a_n(t)|^2>_p=\int\frac{dydz}{2\pi}|a_n(y,z,t)|^2\exp\left(-\frac{y^2+z^2}{w^2}\right)$ of a pump wave is presented. In the early stage of PDI one can see an exponential growth of the energy of primary plasmons with the growth rate being adequately described by the analytical equation (13) (short dotted line). When the energy of primary plasmons is large enough so that the threshold of the secondary decay instability appears to be overcome, the energy of secondary plasmons starts to grow as well. Eventually, the energies of primary and secondary plasmons achieve their saturation levels. It is seen that the saturation levels of the daughter plasmons derived analytically (equation (14) – lower thin dashed horizontal line, equations (15) and (16) – upper thin dashed horizontal lines which are merged) are in a reasonable agreement with the results of numerical modeling.

The power transferred to the UH plasmons at the pump power well above the threshold ($P_0>>P_0^{th}$) can be estimated based on expressions for the number of plasmons at the PDI saturation (14)-(16) and assuming

their diffractive losses from the decay region. The corresponding estimation takes a form $\Delta P \propto (|a_n^s|^2 + |a_m^s|^2 + |a_p^s|^2)/\tau \propto |v_0|^2$. Therefore, we can conclude that the anomalously absorbed power should be proportional to the pump power and thus the anomalous absorption rate $\Delta P / P_0$ at large threshold excess should be constant. This conclusion is confirmed by the results of numerical solution which predicts at the pump power much larger than the PDI power threshold, $P_0^{th} = 5$ kW, the anomalous absorption of X - mode wave at a level of 18%, independently on the pump power. Thus, for the parameters under consideration up to 110 kW are transferred to the daughter UH waves. Subsequently, this power fraction is deposited into the electron component far from the pump wave second harmonic electron cyclotron resonance layer. This can make the power deposition profile much wider than it is predicted by the linear theory and can create an illusion of the fast electron energy redistribution. In other words, this nonlinear absorption mechanism can be responsible, at least partly, for the so-called nonlocal electron transport in the on-axis X2-mode ECRH experiments at T-10 and LHD [12,13]. We can also estimate the pump power fraction absorbed by the daughter IB waves as $\Delta P_1 = 6.3$ kW. The anomalous absorption leads to the generation of a population of the suprathermal ions. Thus, the proposed mechanism can explain the experimental observations of the ion acceleration in the on-axis X2-mode ECRH experiments at TCV and TJ-II [7-10].

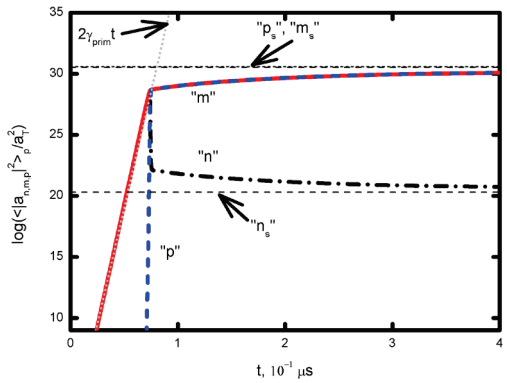


Fig. 1. Temporal evolution of the average number of daughter plasmons given in the logarithmic scale; "n" – $<|a_n(t)|^2>_p / a_T^2$ (dashed dotted line), "m" – $<|a_m(t)|^2>_p / a_T^2$ (solid line), "p" - $<|a_p(t)|^2>_p / a_T^2$ (dashed line); "$n_s$" – equation (14) (lower thin dashed horizontal line), "$m_s$" and "$p_s$" - equation (15) and equation (16) (merged upper thin dashed horizontal lines). The gain coefficient $2\gamma t$ (short dotted line) of the primary decay waves (13).

The nonlinear coupling of different UH waves can lead to the generation of microwave signals with the frequencies smaller than the pump frequency. In this way the proposed nonlinear mechanism explains in detail the anomalous backscattering effect observed at TEXTOR [2]. In particular, the frequency spectrum structure and the spectral power density of the backscattering signal predicted by this theoretical model appear to be in a reasonable agreement with those measured by the ECE and CTS techniques [2,3].

In order to examine the mechanism of anomalous absorption described in this section the model experiment on the linear device "Granite" in Minsk was proposed and then performed [18]. The huge anomalous absorption of microwave power was observed in the plasma column when the density was close to the UHR value for half the pump frequency which validates the main theoretical predictions concerning the possibility of the low-power-threshold two-UH-plasmon PDI of extraordinary wave and its role in the energy balance.

Summarizing, we would like to emphasize that there are two key points of the model developed. The first point is the trapping of the UH waves at the local maximum of a nonmonotonic density profile. The second one of them is the possibility of an additional localization of the UH waves propagating in the opposite directions on the magnetic surface within the spot of a finite-width pump beam. In the forthcoming section we consider the possibility of low-power-threshold ordinary wave decay into a low hybrid wave (LH) and a radially trapped UH wave. We demonstrate that even one radially trapped UH daughter wave can be nonlinearly localized on the magnetic surface due to the finite-width pump, that leads to excitation of the most dangerous absolute PDI.

## 2.2. Low-threshold parametric decay of an ordinary wave

In this section we analyse the low-threshold PDI of an obliquely propagating ordinary wave. The parametric decay leads to the excitation of the obliquely propagating LH wave and the UH wave. The latter appears to be 3D localized due to the nonmonotonic density profile and the finite-width beam. We analyze also the transition of primary PDI to the saturation regime due to the secondary decay instability of primary UH wave. We focus on the case of the one-step down-conversion leading to the low-threshold excitation of the IB and radially trapped UH waves. We derive a set of equations describing the cascade of decays and then solve it numerically under the conditions similar to the on-axis O1-mode ECRH experiments at FTU [6] in which the nonmonotonic density profile arises due to the density pump-out effect from the ECR layer.

The pump ordinary wave can be represented by means of the WKB approximation as follows

$$\mathbf{E} = \mathbf{e}(x) A_0 \exp\left(i\int^x k_x(x', k_z)dx' + ik_z z - i\omega_0 t\right)/2 + c.c. \quad (17)$$

where $\mathbf{e}$ is a polarization vector with its components $e_x / e_y = -i\omega_{ce}/\omega_0$ and $e_x / e_z \approx \sqrt{\eta}\, k_z c/\omega_0$, $\eta$ is the parallel component of the cold-plasma dielectric tensor, $A_0$ is the amplitude defined already in (8) and $k_x \approx \omega_0\sqrt{\eta}\left(1 - k_z^2 c^2/2\omega_0^2\right)/c >> k_z$. A set of equations describing the primary decay of the pump wave (17)

with the fixed amplitude $A_0$ and subsequent secondary decay of the trapped UH wave reads

$$\hat{D}(\varphi_1)=\kappa_p^{2*}\frac{A_0^*}{2H}\varphi_2-\kappa_s^{2*}\frac{|e|}{2T_e}\varphi_1'^*\varphi_2'$$
$$\hat{D}(\varphi_2)=\kappa_p^{2}\frac{A_0}{2H}\varphi_1 \qquad (18)$$
$$\hat{D}(\varphi_1')=\kappa_s^{2*}\frac{|e|}{2T_e}\varphi_1^*\varphi_2'$$
$$\hat{D}(\varphi_2')=\kappa_s^{2}\frac{|e|}{2T_e}\varphi_1'\varphi_1$$

where $\varphi_1\propto\exp(i\omega_1 t)$ and $\varphi_2\propto\exp(-i\omega_2 t)$ are the potentials of primary UH and LH waves, $\varphi_1'\propto\exp(-i\omega_1' t)$ and $\varphi_2'\propto\exp(i\omega_2' t)$ are the potentials of secondary UH and IB waves. In equations (18) the amplitude of pump wave $A_0$ is assumed to be fixed, the integral operators on their left-hand-sides are determined in the same way as in (3), $\kappa_p^2$ and $\kappa_s^2$ are the coupling coefficients of the waves involved in the primary and secondary decays presented explicitly in [20] and [24], correspondingly. Assuming the nonlinear coupling is weak we treat the set of equations (18) using the perturbation procedure [23]. In its first step we neglect the nonlinear pump. The solutions of homogeneous equations describing the trapped UH waves can be presented in the following form

$$\varphi_1=C_n\phi_n(\mathbf{r})\exp(i\omega_n t)+c.c.,$$
$$\varphi_1'=C_m\phi_m(\mathbf{r})\exp(iq_{1z}'z-i\omega_m t)+c.c. \qquad (19)$$

where $C_{n,m}=\text{const}$, the eigenfunctions $\phi_{n,m}(x)$ and eigenfrequency $\omega_{n,m}$ are derived by means of the WKB approximation in the same way as in equations (6) and (7). The choice $q_{1y,z}=0$, $q_{1y}'=0$ allows us to minimize the energy losses of UH plasmons from the decay region. Then, we treat equations in (18) describing the daughter LH and IB waves. Utilizing the perturbation procedure we neglect their right-hand-sides and seek the solution of homogeneous equations by means of the WKB approximation

$$\varphi_2=\frac{C_1}{|D_{2q}(x)|^{1/2}}\exp\left(i\int^x q_{2x}(\omega_2,q_{2z},x')dx'+iq_{2z}z-i\omega_2 t\right)$$
$$\varphi_2'=\frac{C_1'}{|D_{2q}'(x)|^{1/2}}\exp\left(i\int^x q_{2x}(\omega_2',q_{2z}',x')dx'+iq_{2z}'z+i\omega_2' t\right) \qquad (20)$$

where the amplitudes $C_1, C_1'$ are constant, $q_{2x}(\omega_2,q_{2z})$, $q_{2x}'=q_{2x}(\omega_2',q_{2z}')$ are the solutions of the local dispersion relations $D(\omega_2)=0$ and $D(\omega_2')=0$, $q_{2z}=k_z$, $q_{2z}'=q_{1z}'$. The choice $q_{2y},q_{2y}'=0$ minimizes the low frequency waves energy losses perpendicular to the magnetic field along the axis $\mathbf{e}_y$. The pre-exponential factors $\propto 1/|D_{2q}(x)|^{1/2}$, $\propto 1/|D_{2q}'(x)|^{1/2}$ with $D_{2q}$ and $D_{2q}'$ being defined as follows $D_{2q}=\partial D/\partial q_x|_{q_{2x}(\omega_2,x),\omega_2}$, $D_{2q}'=\partial D/\partial q_x|_{q_{2x}(\omega_2',x),\omega_2'}$ ensure the conservation of the wave energy fluxes along the direction of inhomogeneity.

In the second step of the perturbation procedure we take into account the nonlinear wave coupling. The nonlinear three-wave interactions lead to the variation of amplitudes $C_{n,m}$ and $C_1, C_1'$ in such a way that $C_1, C_1'\to C_1(\mathbf{r}), C_1'(\mathbf{r})$ and $C_{n,m}\to C_{n,m}(t,y,z)$. Using the envelope amplitude method we can get a set of the coupled equations

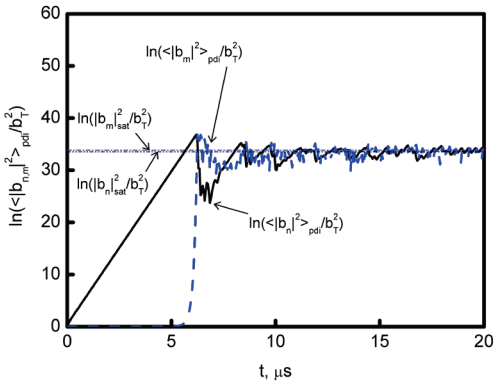


Fig. 2. Temporal evolution of the averaged density of the primary (solid curve) and secondary (dashed curve) UH plasmon energies given in the logarithmic scale. The dash dotted line is $2\nu_{0,0}t$ with $\nu_{0,0}$ determined in (31), the dash-dot-dotted curve is the dependence (35). Two horizontal lines (visually merged) are the saturation levels (36) and (37).

$$\left(\upsilon_{1x}\frac{\partial}{\partial x}+i\Lambda_{1y}\frac{\partial^2}{\partial y^2}+\upsilon_{1z}\frac{\partial}{\partial z}\right)C_1(\mathbf{r})= \qquad (21)$$
$$-\kappa_p^2\frac{|D_{2q}|^{1/2}}{D_{2\omega}}\frac{A_0}{2H}C_n\phi_n(x)\exp\left(i\int^x(k_x-q_{2x})dx'\right),$$

$$\left(\frac{\partial}{\partial t}+i\Lambda_{my}\frac{\partial^2}{\partial y^2}+i\Lambda_{nz}\frac{\partial^2}{\partial z^2}\right)C_n=$$
$$\frac{\kappa_p^{2*}}{D_{n\omega}}\frac{A_0^*}{2H}\int_{-\infty}^{\infty}\frac{dx}{|D_{2q}|^{1/2}}\phi_n^*(x)C_1(\mathbf{r})\exp\left(i\int^x(q_{2x}-k_x)dx'\right)- \qquad (22)$$
$$i\frac{|e|}{2T_e}\frac{\kappa_s^{2*}}{D_{n\omega}}C_m^*\int_{-\infty}^{\infty}\frac{dx}{|D_{2q}'|^{1/2}}\phi_n^*(x)\phi_m^*(x)C_1'(\mathbf{r})\exp\left(i\int^x q_{2x}'dx'\right),$$

$$\left(\upsilon_{1x}'\frac{\partial}{\partial x}+i\Lambda_{1y}'\frac{\partial^2}{\partial y^2}+\upsilon_{1z}'\frac{\partial}{\partial z}\right)C_1'(\mathbf{r})= \qquad (23)$$
$$i\kappa_s^2\frac{|e|}{2T_e}\frac{|D_{2q}'|^{1/2}}{D_{2\omega}'}C_nC_m\phi_n(x)\phi_m(x)\exp\left(-i\int^x q_{2x}'dx'\right),$$

$$\left(\frac{\partial}{\partial t}+i\Lambda_{my}\frac{\partial^2}{\partial y^2}-\upsilon_{mz}\frac{\partial}{\partial z}\right)C_m=$$
$$\frac{i|e|}{2T_e}\frac{\kappa_s^{2*}}{D_{m\omega}}C_n^*\int_{-\infty}^{\infty}\frac{dx}{|D_{2q}'|^{1/2}}\phi_m^*(x)\phi_n^*(x)C_1'(\mathbf{r})\exp\left(i\int^x q_{2x}'dx'\right) \qquad (24)$$

where $\upsilon_{1x,z}$, $\upsilon_{1x,z}'$, $\Lambda_{1y}$ and $\Lambda_{1y}'$ are the local group velocity components and the diffraction coefficient of the daughter LH and IB waves, $\Lambda_{ny,z}$ are the coefficients describing the primary UH waves diffraction in the corresponding directions averaged over the localization region, $\Lambda_{my}$, $\upsilon_{mz}$ are the averaged diffraction coefficient

and group velocity of the secondary UH wave, $D_{n,m\omega} = <\partial D/\partial\omega>_{\omega_{n,m}}$, $D_{1\omega} = |\partial D/\partial\omega|_{\omega_2}$, $D'_{1\omega} = |\partial D/\partial\omega|_{\omega'_2}$. The averaging procedure of an arbitrary function is determined as in equation (11). For the parameters under consideration $(w/l_d)(\upsilon_{1x}/\upsilon_{1z}) \approx 2.1$, $(w/l'_d)(\upsilon'_{1x}/\upsilon'_{1z}) \approx 5.3$ where $l_d = |d\Delta K/dx|^{-1/2}_{x_d}$ and $l'_d = |d\Delta K'/dx|^{-1/2}_{x'_d}$ are the lengths of the three-wave resonance layers and $x_d$, $x'_d$ are the points where the decay conditions hold. Therefore the convective losses of low frequency waves from decay regions across the magnetic field are dominant and we can neglect all terms on the left-hand-side of equations (15), (17) apart from those proportional to the $x$ - derivatives. Then, we integrate (21) and (23) with the boundary conditions $C_1|_{x\to-\infty} = 0$ and $C'_1|_{x\to\infty} = 0$ that yields

$$C_1 = C_n \frac{\kappa_p^2 A_0}{2H} \int_{-\infty}^{x} \frac{d\xi}{|D_{2q}|^{1/2}} \phi_n(\xi) \exp\left(i\int^{\xi}(k_x - q_{2x})dx'\right)$$
$$C'_1 = -i\kappa_s^2 \frac{|e|C_n C_m}{2T_e} \int_{x}^{\infty} \frac{d\xi}{|D'_{2q}|^{1/2}} \phi_n(\xi)\phi_m(\xi) \exp\left(-i\int^{\xi} q'_{2x}dx'\right) \quad (25)$$

Substituting (25) into the right-hand-sides of (22), (24) and introducing the dimensionless functions

$$b_{n,m} = |C_{n,m}| \left(\frac{\omega_{n,m}}{16\pi} D_{n,m\omega}(\omega_{n,m})\right)^{1/2} \quad (26)$$

we arrive at a system of equations for UH waves

$$\left(\frac{\partial}{\partial t} + i\Lambda_{ny}\frac{\partial^2}{\partial y^2} + i\Lambda_{nz}\frac{\partial^2}{\partial z^2}\right) b_n = \left(\gamma_0 \exp\left(-\frac{y^2}{w^2} - \frac{z^2}{w^2}\right) - \gamma'_0(b_m)\right) b_n$$
$$\left(\frac{\partial}{\partial t} + i\Lambda_{my}\frac{\partial^2}{\partial y^2} - \upsilon_{mz}\frac{\partial}{\partial z}\right) b_m = \gamma'_0(b_n) b_m \quad (27)$$

where

$$\gamma_0 = \frac{|\kappa_p^2||A_0|^2}{4H^2 D_{n\omega}|D_{1q}|} \int_{-\infty}^{\infty} dx \int_{-\infty}^{x} d\xi \varphi_n(x)^* \varphi_n(\xi) \exp\left(i\int_{\xi}^{x}(q_{2x} - k_x)dx'\right),$$
$$\gamma'_0(b_{n,m}) = \frac{|\kappa_s^2|^2}{n_e T_e} \frac{|b_{n,m}|^2}{\omega_E^{n,m} D_{n\omega} D_{m\omega} |D_{1q}(x)| r_{de}^2} \times$$
$$\int_{-\infty}^{\infty} dx \varphi_n^*(x)\varphi_m^*(x) \int_{x}^{\infty} d\xi \varphi_n(\xi)\varphi_m(\xi) \exp\left(i\int_{\xi}^{x} q'_{2x}dx'\right)$$

and $r_{de}$ is the Debye length. The parametric decay instability starts with the stage of exponential growth in which the amplitude of primary wave is still small and the secondary decay is yet not excited. In this case the system of equations (27) reduces to the following equation

$$\left(\frac{\partial}{\partial t} + i\Lambda_{ny}\frac{\partial^2}{\partial y^2} + i\Lambda_{nz}\frac{\partial^2}{\partial z^2}\right) b_n = \gamma_0 \exp\left(-\frac{y^2}{w^2} - \frac{z^2}{w^2}\right) b_n \quad (28)$$

Solving it we readily get the exponentially growing solution which is presented as

$$b_n(t,y,z) = b_T \exp\left(\nu_{p,s}t + i\delta\omega_{p,s}t\right)\psi_p(y)\psi_s(z), \quad (29)$$

$$\psi_p(\xi) = \exp\left(-\frac{\xi^2}{2\delta_\xi^2}\right) H_p\left(\frac{\xi}{\delta_\xi}\right), \quad \xi = y, z \quad (30)$$

are the eigenfunctions, $H_p$ is the Hermitian polynomials and $\delta_\xi = \Lambda_{E\xi}^{1/4} w^{1/2} \exp(-i\pi/8 - i\arg\gamma_0/4)/\sqrt[4]{\gamma_0}$ and

$$\begin{pmatrix}\nu_{p,s}\\ \delta\omega_{p,s}\end{pmatrix} = \begin{pmatrix}\mathrm{Re}(\gamma_0)\\ \mathrm{Im}(\gamma_0)\end{pmatrix} -$$
$$\begin{pmatrix}\cos(\arg(\gamma_0/2) - \pi/4)\\ \sin(\arg(\gamma_0/2) - \pi/4)\end{pmatrix} \sqrt{|\gamma_0|} \left((2p+1)\sqrt{\frac{\Lambda_{ny}}{w^2}} + (2s+1)\sqrt{\frac{\Lambda_{nz}}{w^2}}\right) \quad (31)$$

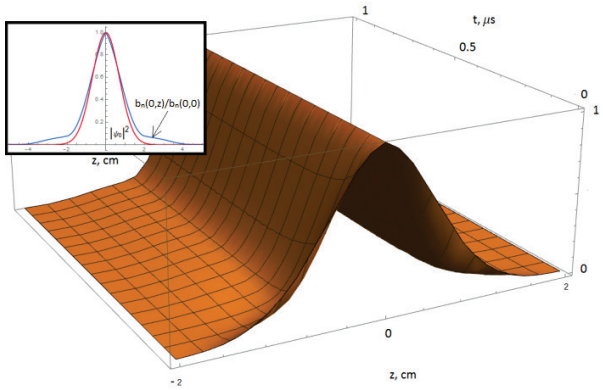


Fig. 3. The spatial distribution of UH wave $|b_n(0,z)|^2/|b_n(0,0)|^2$. Zoom gives the comparison of the function derived numerically with the analytical dependence (30).

The PDI power-threshold $P_0^{th}$ corresponding to the imaginary part of the eigen frequency being equal to zero is determined by the balance between the diffractive loss of UH waves ($\Lambda_{ny,z}/w^2$) and the effectiveness of their nonlinear generation ($\mathrm{Re}(\gamma_0)$). It can be found out solving the following equation

$$\mathrm{Re}\left(\gamma_0\left(P_0^{th}\right)\right) = \cos\left(\arg\left(\gamma_0\left(P_0^{th}\right)/2\right) - \pi/4\right) \times$$
$$\sqrt{\left|\gamma_0\left(P_0^{th}\right)\right|}\left((2p+1)\sqrt{\frac{\Lambda_{ny}}{w^2}} + (2s+1)\sqrt{\frac{\Lambda_{nz}}{w^2}}\right) \quad (32)$$

Thus, the primary decay of the pump ordinary wave (17) leads to the nonlinear transfer of pump power to the localized UH wave (29). It enhances the UH fluctuations up from the thermal-noise-level

$$b_T = \sqrt{\frac{T_e}{\pi w^2}} \quad (33)$$

to such a level $|b_n|$ that the inequality

$$\gamma'_0(|b_n|) \geq \max\left(\frac{\Lambda_{my}}{\pi w^2}, \frac{\upsilon'_{mz}}{w}\right) \quad (34)$$

holds and the power threshold of secondary PDI appears to be overcome. Then, the UH wave $b_n$ starts not only to grow due to the primary instability but at the same time to transfer a part of pump power to the secondary wave. When the secondary PDI power threshold is exceeded significantly, the temporal gain coefficient can be estimated as follows

$$\ln\left(<|b_m(t)|^2>_{pdi}/b_T^2\right) \approx \gamma'_0\left(<|b_n(t)|^2>_{pdi}\right)/\gamma_0 \quad (35)$$

where the averaging procedure over the spot in which the decay occurs is defined as in equation (11). If the PDI saturation results in a stationary regime, the saturation levels of daughter waves can be estimated assuming the nonlinear pumping in the primary decay is balanced by the energy losses due to the secondary decay $\gamma_0 = \gamma'_0(|b_m|_{sat})$ and the pumping in the secondary

decay $\gamma_0'\left(|b_n|_{\text{sat}}\right)$ is compensated by the effect of the secondary wave energy loss from the spot of a pump beam. Finally, we get

$$|b_m|^2_{\text{sat}} = \frac{\gamma_0}{\omega_n}\varepsilon_{\text{T}}, \tag{36}$$

$$|b_n|^2_{\text{sat}} = \max\left(\frac{\Lambda_{my}}{\pi w^2 \omega_m}, \frac{\upsilon_{mz}}{w\omega_m}\right)\varepsilon_{\text{T}}, \tag{37}$$

$$\varepsilon_{\text{T}} = \frac{n_e T_e}{|\kappa_s^2|^2} \frac{\omega_n D_{n\omega}\omega_m D_{m\omega}\left|D'_{2q}\right| r_{\text{de}}^2}{\int_{-\infty}^{\infty} dx \int_x^{\infty} d\xi \varphi_n^*(x)\varphi_m^*(x)\varphi_n(\xi)\varphi_m(\xi)\exp\left(i\int_\xi^x q_{2x}(\omega_2', x')dx'\right)}.$$

Then, we can determine the fraction of anomalous power absorbed by the daughter decay waves as follows

$$\Delta P_{\text{E}} \approx \frac{\Lambda_{nz}}{\pi w^2}|b_n|^2_{\text{sat}} + \frac{\upsilon_{mz}}{\sqrt{\pi} w}|b_m|^2_{\text{sat}} \tag{38}$$

In (38) we have assumed that at the dominant losses of primary and secondary waves from the pump spot are along the magnetic field. It is worth noting that the pump power absorbed by secondary plasmons (the second term in (38)) should be proportional to the pump power, whereas the power fraction absorbed by primary plasmons is not dependent on it. Therefore well above the PDI threshold $P_0 >> P_0^{th}$ the second term in (38) dominates and the fraction absorbed anomalously is proportional to the pump power $\Delta P_{\text{E}} \propto P_0$.

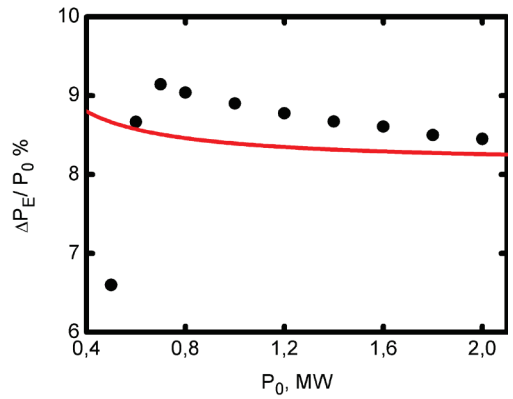


Fig. 4. The anomalous absorption rate derived numerically (scattered symbols) and predicted by the asymptotic equation (38) valid at $P_0 >> P_0^{th}$ are shown; $P_0^{\text{th}} = 125$ kW.

Then, we solve equations (27) numerically in a 2D box $2y_B \times 2z_B$. We impose the periodic boundary conditions improving stability of the numerical scheme. The initial conditions for the UH wave amplitudes are assumed to be determined by the thermal-noise level $|b_{n,m}(0)| = b_{\text{T}}$ (see (33)), whereas their spatial distribution is supposed to be homogeneous. Solving for the incident pump power $P_0 = 600$ kW and $w = 1$ cm beam we get the dependences which are shown in figure 2. In it one can see the temporal evolution of the averaged density of the primary (solid curve) and secondary (dashed curve) UH plasmon energies given in the logarithmic scale. In the early stage of primary decay going on approximately up to 6 μs the growth of the primary UH wave energy is perfectly described by the analytical dependence $2\nu_{0,0}t$ shown by the dash-dotted line with $\nu_{0,0}$ having been determined in (31). For the parameters under consideration the growth-rate is $2\nu_{0,0} = 5.9$ MHz and the power threshold of primary decay is $P_0^{\text{th}} = 125$ kW. In this regime the primary daughter wave retains its spatial distribution invariable (see figure 3). As it is shown in a zoom in figure 3 it is well described by the analytical dependence (30). When the secondary PDI power threshold is exceeded the energy of secondary wave (dashed curve) starts to grow. The growth is reasonably described by the analytical dependence (35). Then, we can see the temporal relaxation of the strong nonlinear phenomenon and the transition of the instability into the saturation regime. The saturation levels of the daughter waves are quite well described by the analytical estimations (36) and (37), at least in the logarithmic scale. Then, we can calculate the daughter waves total energy

$$W_{\text{d}} = \int_{-y_B}^{y_B} dy \int_{-z_B}^{z_B} dz\left(|b_n(y,z)|^2 + |b_m(y,z)|^2\right) \tag{39}$$

Finding the temporal derivative of the dependence (39) in the saturation regime, which appears to be linear, allows us to estimate the power fraction gained by the daughter UH waves at the level $\Delta P_{\text{E}} \approx 52$kW. Subsequently, this power fraction is deposited into the electron component far from the pump wave absorption region predicted by linear theory. We can also estimate the pump power fraction absorbed by the LH and IB waves $\Delta P_{\text{I}} = 0.9$ kW. This anomalous absorption can lead to the generation of a population of the suprathermal ions. In figure 4 the anomalous absorption rate derived numerically (scattered symbols) and predicted by the asymptotic equation (38) valid at $P_0 >> P_0^{th}$, $P_0^{\text{th}} = 125$kW are depicted. As it is seen, the model developed in this paper predicts at the high pump power anomalous absorption rate of 8.4 %. This value is lower than in the case of the X-mode decay producing UH plasmons analysed in [21] due to the specific direction of the pump electric field (almost parallel to the magnetic field). The low value of the anomalous absorption rate provides an argument in favour of omitting the pump depletion in our analysis.

## 3 Conclusions

We have described the theoretical model, which interprets the anomalous phenomena experimentally observed in the X2-mode and O1-mode ECRH experiments, such as the generation of backscattering signals and the fast ion generation, as a consequence of the low-threshold PDI of a pump wave leading to generation of localized UH daughter waves in presence of a nonmonotonic (hollow) density profile. The natural consequence of this model is also the absolute instability excitation in presence of a finite-width pump beam and its saturation at a substantially high level due to the secondary decay phenomena and the pump depletion. The developed model also results in the anomalous pump wave absorption at a level of 10% or higher.

We have investigated the X2-mode wave decay into two 3D localized UH waves and analysed the

transition of primary instability into the saturation regime due to both the pump wave depletion and the secondary decays of daughter UH wave, leading to the excitation of secondary IB/LH and UH waves. The threshold of this spontaneous parametric frequency down-conversion is shown to be easily overcome for the secondary UH waves trapped at the local maximum of a density profile. The model predicts substantial RF power transfer to the UH waves (up to 25%). Subsequently, the UH waves power is deposited into the electron component far from the pump wave electron cyclotron resonance layer. This makes the power deposition profile much wider than it is predicted for the pump wave itself. The anomalous absorption of the pump power by the IB or LH waves leads to the generation of a population of the suprathermal ions, which can explain the experimental observations of the ion acceleration in the X2-mode ECRH experiments at TCV and TJ-II [7-10].

Nonlinear coupling of different UH waves can lead to the generation of microwave signals at frequencies smaller than the pump frequency. Thus, the nonlinear mechanism allows explaining the anomalous backscattering effect observed at TEXTOR [2] in detail. In particular, the frequency spectrum structure and the spectral power density of the backscattering signal predicted by this theoretical model appear to be in a reasonable agreement with those measured by the ECE and CTS techniques [2,3].

We have also investigated the pump O-mode wave anomalous absorption due to the parametric excitation of trapped UH waves. The instability power threshold ( $P_0^{\text{th}} = 125$ kW ) can be exceeded by the MW microwave beams utilized usually for auxiliary heating in the O1-mode ECRH experiments. However, its growth-rate is much smaller than the growth-rate of X-mode PDI. This is due to the weak coupling of the ordinary wave to the electrostatic waves. Nevertheless, the derived growth-rate of O-mode PDI is large enough allowing this nonlinear phenomenon to play an important role in the ECRH power balance. In order to estimate the fraction of pump power absorbed anomalously we have analyzed the saturation regime of primary instabilty. We assumed the UH wave secondary decay into the localized UH waves and IB waves to be a presumably most important nonlinear mechanism responsible for the transition to saturation regime. We have estimated the power fraction gained by the daughter UH waves in the O1-mode ECRH experiments at FTU, in which the 600 kW pump beams are utilized. Numerical solution gives the power fraction $\Delta P_{\text{E}} \approx 52$kW absorbed via the UH daughter waves. This power fraction is deposited into the electron component far from the pump wave absorption region predicted by linear theory.

It is worth noting that the powerful ECRH utilizing ordinary waves is planned for application in ITER. It should allow the neoclassical tearing mode control leading to reduction of its influence on the confinement in this thermonuclear reactor. According to the analyses performed in this paper, if the nonmonotonic density profile will arise in ITER at the edge of the discharge, the low-threshold parametric decay of the pump wave to the 3D localized UH wave could be possible playing a role in the ECRH power balance. This stimulates further analysis of the O1-mode parametric decay under the conditions which will be typical for ITER.

*The financial support of the Ioffe Institute is acknowledged.*

1. M. Porkolab, B. I. Cohen, Nucl. Fusion **28**, 239 (1988)
2. E. Westerhof, S. Nielsen, J. W. Oosterbeek, *et al.*, Phys. Rev. Lett. **103**, 125001 (2009)
3. S. K. Nielsen, M. Salewski, E. Westerhof, et al., Plasma Phys. Control.Fusion **55**, 115003 (2013)
4. S. Kubo, M. Nishiura, K. Tanaka et al., Rev. Sci. Instrum. **81**, 10D535 (2010)
5. W. A. Bongers, W. Kasparek, N. Doelman et al., EPJ Web Conf. **32**, 03006 (2012)
6. A. Bruschi, E. Alessi, W. Bin et al., Nucl. Fusion **57**, 076004 (2017)
7. A. N. Karpushov, S. Coda, and B. P. Duval, Proc.of 33rd EPS Conference **30I**, P–1.152 (2006)
8. S. Coda for the TCV Team, Nucl. Fusion **55**, 104004 (2015)
9. D. Rapisarda, B. Zurro, V. Tribaldos et al., Plasma Phys. Controlled Fusion **49**, 309 (2007)
10. B. Zurro, A. Baciero, V. Tribaldos et al., Nucl. Fusion **53**, 083017 (2013)
11. M. Martínez, B. Zurro, A. Baciero et al., Plasma Phys. Control. Fusion **60,** 025024 (2018)
12. V. F. Andreev, A. A. Borschegovskij et al., Plasma Phys. Control. Fusion **58**, 055008 (2016)
13. N. Tamura, S. Inagaki, K. Ida et al., Proc. 3rd EFDA Transport Topical Group Meeting O5-03 (2010)
14. A. Yu. Popov, E. Z. Gusakov, Plasma Phys. Control. Fusion **57**, 025022 (2015)
15. A. Yu. Popov, E. Z. Gusakov, European Phys. Lett. **116**, 45002 (2016)
16. E. Z. Gusakov, A. Yu. Popov, Plasma Phys. Control. Fusion **59**, 025005 (2017)
17. E. Z. Gusakov, A. Yu. Popov, Physics of Plasmas **23**, 082503 (2016)
18. L. V. Simonchik, A. B. Altukhov, *et al.*, EPJ Web of Conferences **149**, 03013 (2017)
19. E. Z. Gusakov, A. Yu. Popov *et al.*, Plasma Phys. and Control. Fusion **59**, 075002 (2017)
20. E. Z. Gusakov, A. Yu. Popov, Physics of Plasmas **25**, 012101 (2018)
21. E. Z. Gusakov, A. Yu. Popov, Plasma Phys. Control. Fusion **60**, 025001 (2018)
22. D. G. Swanson, Plasma Waves Academic Press, Boston (1989)
23. E. Z. Gusakov, V. I. Fedorov, Sov. J. Plasma Phys. **5**, 463 (1979)
24. E. Z. Gusakov, A. Yu. Popov, Journal of Experimental and Theoretical Physics **127**, 155–166 (2018)